PSIM simulations of a dc SQUID magnetometer

1. INTRODUCTION

A superconducting quantum interference device (SQUID) is considered the most sensitive of all known magnetometers, capable of measuring magnetic fields in the femto Teslas (fT) range, as reported by Faley *et al*. (2002). Such weak magnetic fields need to be detected for biomagnetic and space weather applications (NOAA Space WeatherPrediction Center). Regions of the Van Allen radiation belt (VARB) closer to the Earth surface are characterised by weak Earth's magnetic fields, which results in a phenomenon called the South Atlantic Magnetic Anomaly (SAMA). This occurrence constitutes space weather storms, which degrades any orbiting spacecraft (Acuna, 2002; Lanzerotti, 2000). A highly sensitive magnetometer is therefore needed to study this phenomenon, and to acquire useful data that will improve the existing models used for space weather predictions. Any commercial-off-the-shelf SQUID magnetometer is quite expensive to acquire, and can be easily damaged during test analysis. Hence, there is need for predicting the magnetometer's behavior, through simulation, before subjecting it to real life experiment.

The simulation package used is the PSIM simulation software from Powersim Inc. PSIM is a fast and user friendly power electronics and motor control simulation package. It consists of three entities – SIMCAD, for circuit schematic editor; PSIM, for simulation; and SIMVIEW, for waveform processing (Powersim, 2001). This package was selected for this study, because, it provides a means of simulating SQUIDs without the need for the superconducting simulation tools, which may not be easily accessible. PSIM has fast simulation capability, together with an added advantage of being able to simulate the thermal noise effects of the SQUID magnetometer.

Preliminary knowledge of Josephson junctions and dc SQUID magnetometers is presented in section 2. Section 3 presents a comprehensive description of a Josephson junction model and a dc SQUID magnetometer model. The simulations of these models are then described in section 4, with their results presented therein. The paper is then concluded in section 5.

2. THE JOSEPHSON EFFECT AND SQUID MAGNETOMETER THEORY

The history of superconductivity dates back to the year 1911 when Kamerlingh Onnes cooled a mercury sample with liquid Helium-4 (^{4}He). Helium boils at 4.2 K (HyperPhysics, 2000). The sample's resistance dropped sharply to a value close to zero. This later gave birth to the technology behind the SQUID magnetometer's operation, discovered by Brian Josephson in 1962. A superconducting (critical) tunneling current was discovered to flow between two superconductors, separated by a thin layer of insulation, in the absence of any applied voltage (Daniel, 1998). This separation layer is called the Josephson junction. The value of this critical current, I_c, through the Josephson junction is affected by the presence of magnetic fields.

As described in Macintyre (1999), a dc SQUID magnetometer setup consists of the pick-up circuit, SQUID loop, usually made from $YBa_2Cu_3O_{7-x}$ (YBCO), cryogenic cooling system, and feedback electronics. The SQUID loop is composed of two Josephson junctions. The working principle of a typical dc SQUID is clearly depicted in Figure 1 (with the read out electronics). The SQUID is first cooled down to a cryogenic temperature (below 100 K), which is the Josephson junction's transition temperature, T_c, and then biased by applying a dc current, I_b, to its loop. The output voltage across the junctions is a periodic function of the sensed magnetic flux through the pick-up loop, with a period of 1 fluxon or 1 Φ_0 (1 $\Phi_0 = 2.07 \times 10^{-15}$ Wb). The feedback voltage maintains a modulated constant flux magnitude within the SQUID loop, through the feedback coil and a feedback resistor. This feedback circuitry is a flux locked loop (FLL). The output from the integrator presents a linearised response from the SQUID, relative to the sensed flux.

Figure 1: The mode of operation of dc SQUID magnetometers

If I_b to the SQUID is lower than I_c, at T_c, no voltage appears across the SQUID's junctions (van Zyl, 2010). The voltage - current (V - I) characteristic of the Josephson junction, at temperatures lower than T_c, is linear. The behaviour has a flat response at the region where the junction's current is lower than I_c, as depicted in Figure 2. In this case, a resistanceless current is said to flow through the junction. The output voltage, however, starts varying in proportion with the bias current as it exceeds the critical current, I_c. For SQUID magnetometers, the flat region seems to get narrower, as the sensed field increases from $n\Phi_0$ to $(n + 1)\ \Phi_0$, where $n = 0, 1, 2,\ldots,$, and the sequence repeats itself. This shows that the external magnetic fields have a quantum effect on the critical junction current.

Figure 2: The dc SQUID voltage current characteristics in the order of increasing applied flux, from the extreme sides towards the middle

3. MODELLING AND SIMULATION OF A JOSEPHSON JUNCTION

Depending on the method of fabrication, a Josephson junction can be regarded as either a resistively and capacitively shunted junction (RCSJ), or a resistively shunted junction (RSJ). In either case, a capacitive channel and or a resistive channel are seen in parallel to a superconducting channel. The combination of these channels makes up the Josephson junction. The RSJ type is considered here. Details on RCSJ can be found in Clarke and Braginski (2004).

Figure 3 shows the circuit model of an RSJ. As presented by Clarke and Braginski (2004), the super current, I_s, across a Josephson junction is described by Josephson's first equation given in equation (1):

Figure 3: Equivalent circuit of a resistively shunted Josephson junction

$$I_s = I_c \sin(\delta) \tag{1}$$

where δ is the gauge invariant phase difference (GIPD), otherwise called the Josephson phase difference. When magnetic field is applied, a 2π periodic Josephson phase difference develops in the phases of the quantum wave functions across the Josephson junction. This wave function governs the superconducting current in the Josephson junction.

Figure 3 can be used to deduce the effective current through the RSJ as:

$$i = I_c \sin(\delta) + v / R_n \tag{2}$$

Equation (3) gives the second Josephson's equation that expresses the voltage developed across the Josephson junction, if the GIPD is time dependent (Clarke and Braginski, 2004):

$$\frac{d\delta}{dt} = \frac{2\pi}{\Phi_0} v \tag{3}$$

From equations (2) and (3), it follows that

$$i = I_c \sin(\delta) + \frac{1}{R_n} \frac{\Phi_0}{2\pi} \frac{d\delta}{dt} \tag{4}$$

The time dependent voltage, $u(\tau)$, across the junction, normalised by $I_c R_n$ or the characteristic voltage, V_c (i.e., $V_c = I_c R_n$), can be represented by (Clarke and Braginski, 2004):

$$u(\tau) = \left(i_b^2 - 1\right) / \left(i_b + \cos\left(\tau w_c \sqrt{i_b^2 - 1}\right)\right), \quad for I_b > I_c$$
$$= 0 \; otherwise \tag{5}$$

Where,

i_b is the normalised bias current ($i_b = I_b / I_c$)
ω_c is the Josephson junction characteristic frequency ($\omega_c = 2\pi I_c R_n / \Phi_0$)
τ is the normalised time ($\tau = t\,\omega_c$)

As i_b rises above i_c, the excess current flows through the R_n channel and produces an increasing dc voltage across the Josephson junction. The supercurrent in the superconducting channel, in turn, oscillates at ω_c; thereby

decreasing the supercurrent in the entire junction, since the excess current is now being diverted into the R_n channel.

Equation (4) can be compared with the voltage, v_{ind} across an inductor, or the current, i_{cap} across a capacitor. The voltage, v, across the junction is synonymous to the voltage across an inductor, or the current through a capacitor, with the phase, δ, being the inductor's current, or the capacitor's voltage.

i.e,

$$v = \frac{\Phi_0}{2\pi}\frac{d\delta}{dt} \Leftrightarrow v_{ind} = L\frac{di_{ind}}{dt} \tag{6}$$

$$v = \frac{\Phi_0}{2\pi}\frac{d\delta}{dt} \Leftrightarrow i_{cap} = C\frac{dv_{cap}}{dt} \tag{7}$$

Figure 4 is the complete Josephson junction modelled. The PSIM blocks used are used to express the equations that express the theoretical behaviour of a typical Josephson junction. Equations (2) and (7) are modelled using a voltage - controlled current source (see Figure 4). The voltage across the capacitor is used as the phase, δ, processed through a sine block, multiplied with the critical current, I_c (using a proportional block). The result is then used to control another voltage - controlled current source. This current source, whose output represents the voltage across the Josephson junction, is connected in parallel to the Josephson junction's shunt resistor, R_n. The voltage sensor is used to convert any signal at its input to a voltage. The capacitance value is $C = \Phi_0/2\,\pi$.

Figure 4: The PSIM model of a RSJ Josephson junction

Intrinsic white noise is usually generated by Josephson junctions, due to the presence of the shunt resistance, R_n (Burger, 2008). This noise is thus modelled in parallel with the Josephson junction's shunt resistor, R_n (as shown in Figure 4), by using a random current source, whose peak-to-peak value is the rms (root mean square) value of the theoretical noise current given by:

$$i_{rms} = \sqrt{4K_BTB / R_n} \tag{8}$$

Where,

K_B = 1.38 X 10^{-23} J/K (Boltzmann's constant)

T = Operating temperature (77 K for M1000 SQUID)

B = Noise bandwidth (in Hz)

The Josephson junction's parameters used were obtained from (Star Cryoelectronics, 2009), and they are:

I_c = 25 µA (the value ranges from 5 µA, at minimum, to 50 µA, at maximum)
R_n = 6 Ω (junction resistance)
M_f = 0.0588 Φ_0/µA (feedback mutual inductance)

The simulation results in Figure 5 reveal the oscillation of the Josephson junction, by using various constant bias currents, I_b. The curves show that the amplitudes are all the same, representing the characteristic voltage, V_c, of the junction, while the oscillation frequencies, together with the offset voltages (representing the dc voltages), are dependent on the bias current magnitudes. This affirms the interpretation of equation (5), which describes the oscillating nature of the junction.

Figure 5: The simulated Josephson junction's oscillations at steady bias currents (I_b = 1.1 I_c, 2.2 I_c, 4.4 I_c and 8.8 I_c)

The result of the Josephson junction's *V - I* characteristic in Figure 6 shows the effect of the voltage oscillation, which poses a challenge in tracing out the curve. The junction's output is time-averaged, using a 15 MHz low pass filter (shown in Figure 4), in order to remove the Josephson oscillation. Figure 7 shows the output, after filtering. These Figures show that, when the bias current, I_b, is less than I_c, there is no voltage across the junction. As soon as I_b exceeds I_c, the junction's time-averaged voltage rises to V_c from 0 V. The region between 0 and 1, on the "I_b /I_c" axis, represents the Josephson junction's I_c. This affirms the behaviour of a typical Josephson junction, as discussed in section 2.

Figure 6: The simulated Josephson junction showing the unfiltered *V -I* characteristics

Figure 7: The simulated Josephson junction showing the filtered *V -I* characteristics

The effect of thermal noise is also presented in Figure 8. The *V - I* characteristics without noise and the one with an added 500 MHz bandwidth noise are both superimposed. The noise effect is insignificant, because the input current sweep is large (i.e., between -3 I_c and 3 I_c). The noise effect becomes significant, if the bias current is less than the rms value of the thermal noise, as presented in Figure 9. In this simulation, the rms current is i_{rms} = 0.59515 μA, according to equation (8). The *V - I* characteristic, with the bias current swept between – 0.03 I_c and 0.03 I_c, becomes distorted, due to the effect of the noise.

Figure 8: The simulated Josephson junction showing the superimposed *V -I* characteristics, both with and without noise

Figure 9: The simulated Josephson junction showing the distorted *V - I* characteristics, when the bias current is swept between -0.03 I_c and 0.03 I_c

4. MODELLING AND SIMULATION OF A DC SQUID MAGNETOMETER

A dc SQUID magnetometer is formed from the combination of two RSJs. It can thus be modelled by combining two models of the Josephson junction previously described. The SQUID's model equation is similar to equation (4) (Clarke and Braginski, 2004). The equivalent circuit for a RSJ type dc SQUID can be expressed as:

$$i = I_{c,SQ} \sin\delta + \frac{1}{R}\frac{\Phi_0}{2\pi}\frac{d\delta}{dt},$$

but,

$$I_{c,SQ} = 2I_c\left|\cos\left(\pi\,\Phi/\Phi_0\right)\right|$$

where, $Ic_{,SQ}$ is the absolute critical current as a function of the sensed flux, Φ and R is the parallel combination of the two Josephson junction's resistors.

Hence,

$$i = 2I_c\left|\cos\left(\pi\,\Phi/\Phi_0\right)\right|\sin\delta + \frac{1}{R}\frac{\Phi_0}{2\pi}\frac{d\delta}{dt} \tag{9}$$

This forms the basic modeling equation for the SQUID magnetometer. If equation (9) is time-averaged, the voltage across the SQUID's junctions can be expressed as:

$$V = R\sqrt{I_b^2 - 4I_c^2\cos^2(\pi\,\Phi/\Phi_0)} \tag{10}$$

Equation (9) is used in the SQUID simulation. Similar to the Josephson junction's case, this equation is also synonymous to equation (7). It is modelled using a voltage-controlled current source. The flux input to the SQUID, and the π (i.e., 3.142) parameter, according to equation (9), are modelled using the PSIM dc voltage blocks, multiplied, using a multiplication block, and then processed through a cosine block, before finally coupling it to the capacitor's voltage. See Figure 10 for the PSIM model.

Figure 10: The PSIM model of a dc SQUID magnetometer

To consider how the SQUID magnetometer responds to a small input flux, a swept flux of ± 0.5 Φ_0 is used as the input to the magnetometer. Figure 11 shows the corresponding output V - Φ response (without the FLL), which is sinusoidal, with a period of 1 Φ_0. Its response to a large input flux can be observed by using a sinusoidal input flux pattern, with 3 Φ_0 amplitude and 5 kHz frequency. The corresponding output V - Φ response is also sinusoidal, as displayed in Figure 12. A sinusoidal response is as well obtained, when the input flux is swept with ± 3 Φ_0, as seen in Figure 13. Outputs from these two Figures affirm that the SQUID's behaviour is always sinusoidal, regardless of what pattern of change the sensed flux takes. It is, however, difficult to know the magnitude of the sensed flux from this output. This, therefore, calls for the use of a FLL circuit for linearising the SQUID's output. A bias current, $I_b = 3.4\ I_c$, is used to bias the SQUID. This allows the SQUID's response to be fully sinusoidal, thereby making it easy to be linearised.

Figure 11: The simulated resistively shunted junction SQUID output voltage-flux response with a swept input of ± 0.5 Φ_0

Figure 12: The simulated resistively shunted junction SQUID output voltage-flux response with a 3 Φ_0 sinusoidal input at 5 kHz

Figure 13: The simulated resistively shunted junction SQUID output voltage-flux response with a swept input of ± 3 Φ_0

As it can be observed from Figures 11 to 13, the simulated SQUID's response appears relatively linear at every interval between $n\ \Phi_0$ and 0.5 $n\ \Phi_0$. Midway between these regions, is (2 n + 1) Φ_0 /4. This is known as the SQUID's operating point, where the response seems perfectly linear. It is necessary to apply a bias flux of such value to the SQUID, so as to be able to sense small changes, $\delta\Phi$ in the external flux. The slope of a tangent to this point gives the maximum V - Φ transfer coefficient, which represents the SQUID's sensitivity, V_Φ. In this case, V_Φ = 779.2 mV_c / Φ_0, where $V_c = I_c\ R_n$. This sensitivity is needed to compute the SQUID's gain, G_{SQ} (Clarke and Braginski, 2004).

Figure 15 shows the V - I characteristic of the simulated SQUID, in the absence of any external magnetic flux, when the bias current is swept between -3.4 I_c and 3.4 I_c. This result looks like that of the simulated Josephson junction (shown in Figure 7), except that the flat region is $2\ I_c$, instead of I_c. This shows that the SQUID actually contains two Josephson junctions.

Figure 14: The simulated SQUID's V - I characteristics at 0 Φ_0 input flux with no noise introduced

With a 500 MHz bandwidth noise introduced into the SQUID, its effect is insignificant, as clearly shown in Figure 15. This is simply because the current sweep is larger than the rms value of the thermal noise. It is therefore strongly suggested that the SQUID bias current be reasonably high, so as to suppress the thermal noise effect in the Josephson junctions.

Figure 15: The simulated SQUID's V - I characteristics at 0 Φ_0 input flux with a 500 MHz bandwidth noise superimposed

Magnetic fluxes of 0 Φ_0, 0.25 Φ_0 and 1 Φ_0 are applied to the SQUID, in order to show how the maximum critical current (the flat region) is affected by the sensed field. Figure 1 shows the superimposed responses. The flat response is seen to reduce from the maximum value, at 0 Φ_0 (the bold line on the Figure), downwards, as the input flux increases, and back to the maximum, at 1 Φ_0 (bold line on the Figure). This affirms the expected behaviour of the SQUID, when it senses external magnetic fields, as previously discussed in section 2.

Figure 16: Superimposed SQUID's *V - I* characteristics at input fluxes of 0 Φ_0, 0.25 Φ_0 and 1 Φ_0

Figure 17 shows the SQUID's response, whith a bias current, I_b = 15 µA. No voltage is seen across the SQUID, since the bias current is less than the critical junction current. At this state, the entire current applied to the SQUID only accumulates in the superconducting arms of the Josephson junctions. This behaviour confirms the SQUID's attribute discussed in section 2.

Figure 17: The simulated SQUID's voltage response at I_b = 15 µA bias current

5. MODELLING AND SIMULATION OF A FLUX LOCKED LOOP

Presented in Figure 18, is a SQUID magnetometer model (left side of the Figure), composed of mathematical blocks, which are used to mimic the theoretical behaviour of a typical SQUID sensor, according to Equation (9). As established in section 4, the sinusoidal output from the SQUID needs to be linearised, in order to be able to interpret it. A FLL circuitry is used to perform the linearisation function. The right hand side of the Figure is the PSIM model of a FLL (with each component indicated by a dotted rectangular box), directly coupled to the SQUID's output. This comprises of a preamplifier, integrator and a feedback network, with gain, G_{fb}, to the SQUID. The function of the preamplifier is to bring the SQUID's gain to unity. This means the preamplifier gain, A_{preamp}, is the reciprocal of the SQUID's gain, G_{SQ} (Clarke and Braginski, 2004). The integrator integrates the signal, and generates an output, which adds flux to the SQUID, in order to null the integrator's input. In this case, the SQUID is said to be locked.

Figure 18: The PSIM model of the flux locked loop

The parameters used for modelling the FLL circuit are calculated using the parameter equations accessed from Clarke and Braginski (2004), and the manufacturer's specifications provided by Star Cryoelectronics (2009). The simulation is considered for a feedback gain of G_{fb} = 75 Φ_0 /V, f_1 value of 36 MHz (i.e, the unity gain frequency), which yields an integrator with a time constant of 1.224 µs. The SQUID gain is therefore 0.0088, obtained from $G_{SQ} = V_\Phi G_{fb}$, where V_Φ has already been determined in section 4. The dc offset voltage generated by the bias current, I_b has to be compensated for in the FLL circuit. This value is measurable from the bare SQUID output, and it is represented by the V_{offset} block in Figure 18. The input to the feedback loop may not necessarily come from the low pass filter, since the preamplifier and the integrator act as low pass filters. This is because, in reality, the electronics are limited in terms of cut off frequencies, which makes the signals to be filtered, thereby neglecting the need for any low pass filter.

In a practical sense, designing the FLL involves basically the combination of operational amplifier(s) and resistors (for the preamplifier circuit), and the combination of a capacitor, resistors and an operational amplifier (for the integrator circuit). The voltage offset compensator included in the preamplifier (Figure 18) can be achieved by adjusting the voltage offset adjustment of the operational amplifier, depending on the manufacturer's specification. The operational amplifiers should be of high slew rate, high gain bandwidth and low voltage and current noise, with very low input bias current, because the SQUID's bias current is in the µA range. Typical examples of this type of operational amplifier include TL072, OPA657 and OPA134 (Texas Instruments, 2005; Texas Instruments, 2008; Burr-Brown, 1996). The feedback network is mainly composed of a feedback resistor and a feedback inductor, coupled to the SQUID. Practical design and fabrication of directly coupled FLL circuits have been reported (Ogunyanda, 2013; van Zyl, 2010; Burger, 2008). For more sophisticated SQUID readout electronics, the reader is referred to Gershenson (1997), Basso, Perold, and Lourens (1998) and Drung *et al*. (2005).

The modelled FLL is tested, by linearly sweeping the input flux from -12.5 Φ_0 to 0.75 Φ_0. In order to clearly display the FLL's linearising capability, the direct output from the SQUID, (i.e, before coupling it to the FLL circuit), is as displayed in Figure 20 (input displayed as Φ - *time* relation, and output as V - Φ relation). The resulting linearised FLL's output voltage, with respect to the simulation time, is as displayed in the upper part of Figure 20, with a linear slope of 0.83 mV/μs, which represents the slew rate. The lower part of Figure 20 shows the FLL's V - Φ response, with a linear slope of 250.8 mV/ Φ_0, which is the voltage sensitivity. This linearising capability makes it very easy to know the voltage value that corresponds to any external flux.

Figure 19: The SQUID's voltage response to a swept input flux from -12.5 Φ_0 to 0.75 Φ_0, without the flux locked loop

Figure 20: The SQUID's voltage response to a swept input flux from -12.5 Φ_0 to 0.75 Φ_0, using the flux locked loop

The linearity in the FLL's output is relative to the pattern of change in the input flux. This is demonstrated by using non-linear input fluxes to the SQUID. Figure 21 shows the FLL's response to a swept input flux from - 0.25 Φ_0 to 0.75 Φ_0 over 50 ns, and then to – 1.25 Φ_0 over 50 ns. Figure 22 also shows the FLL's response to a sinusoidal input flux of amplitude, 0.5 Φ_0, at 10 kHz. This output signal is also a 10 kHz signal. This clearly shows that the FLL is indeed a linear V - Φ device, which helps the SQUID magnetometer to maintain the sensed flux at the working point.

Figure 21: The flux locked loop's voltage response to a swept input flux from - 0.25 Φ_0 to 0.75 Φ_0 and later to – 1.25 Φ_0

Figure 22: The flux locked loop's voltage response to a sinusoidal input flux of amplitude, 0.5 Φ_0 at 10 kHz

5 CONCLUSIONS

A Josephson junction and dc SQUID magnetometer's characteristics have been simulated with PSIM, with the results presented. The simulation results corroborate the expected behaviour of a typical Josephson junction and dc SQUID magnetometer, with a modulating sinusoidal output voltage, of constant amplitude, V_c, and an offset, $V_{off,}$ depending on the bias current. The V - I characteristics of the Josephson junction and the SQUID magnetometer are seen to represent the expected behaviours, showing the modulating nature of the junction current as the sensed flux varies. Thermal noise contributions due to the junction's resistance are seen to be insignificant, if large bias signals are involved. This implies that the bias current must be reasonably high, in order to suppress the thermal noise effect in the Josephson junctions. The simulations show that the SQUID magnetometer's V – Φ response is periodical, at a period of 1 Φ_0. The modelling of a flux locked loop circuit for linearising the SQUID's output is also presented. The resulting response shows that the external flux can be linearly related to the output voltage, with a slope of 464.1 mV/ Φ_0. For efficient simulation speed, physical circuit components like resistors and capacitors could not be used to build the integrator. Instead, an integrator block was directly used from the PSIM library.

6 ACKNOWLEDGMENTS

I want to appreciate the National Research Foundation, and the Department of Science and Technology for the bursary awarded me during the course of this research.

REFERENCES

Acuna, M.H. (2002), "Space-based magnetometers", *Review of Scientific Instruments*, Vol. 73 No. 11, pp. 3717-3736.

Basso, V.G., Perold, W.J. and Lourens, J.G. (1998), "A dual SQUID linearization concept using a phase modulation scheme", *IEEE Trans. Appl. Supercond.,* Vol. 8 No. 2, pp. 125-131.

Burger, W.A. (2008), "The design and analysis of a dc SQUID for a SQUID microscope", available at: http://scholar.sun.ac.za/handle/10019.1/2239 (accessed 20 September 2011).

Burr-Brown (1996), White Paper on high performance operational amplifiers, Dallas.

Clarke, J. and Braginski, A.I. (2004), *The SQUID handbook: vol. I, fundamentals and technology of SQUIDs and SQUID systems*, Wiley-VCH, Sl Weinheim.

Clarke, J. and Braginski, A.I. (2005), *The SQUID handbook: vol. II, Applications of SQUIDs and SQUID systems*, Wiley-VCH, Sl Weinheim.

Daniel, B.Y. (1998), "Electronic characteristics of SQUIDs", available at: http://dspace.mit.edu/handle/1721.1/10148 (accessed 11 October 2012).

Drung, D. Abmann, C. Beyer, J. Peters, M. Ruede, F. and Schurig, T. (2005), "dc SQUID readout electronics with up to 100MHz closed-loop bandwidth", *IEEE Trans. Appl. Supercond.,* Vol. 15 No. 2, pp. 777-780.

Faley, M.I., Poppe, U., Urban, K., Paulson, D.N., Starr, T.N. and Fagaly, R.L. (2002.), "Sensitive HTS DC-SQUID gradiometers for magnetic evaluation applications", *Physical C*, Vol. 372-376, pp. 217-220.

Gershenson, G. (1997), "Performamnce analysis of modified flux locked loop additional positive feedback SQUID", *IEEE Trans. Appl. Supercond.,* Vol. 7 N0. 1, pp. 23-26.

HyperPhysics (2000), "Liquid Helium", http://hyperphysics.phy-astr.gsu.edu/hbase/lhel.html (accessed 29 October 2012).

Lanzerotti, L.J. (2000), "Space weather effects on communications", in *Daglis I.A. Space storms and space weather hazards Proceedings of the NATO Advanced Study Institute on Space Storms and Space Weather Hazards in Hersonissos, Crete*, 19-29 June, 2000, Kluwer Academic Publishers, Dordretcht, pp. 313-335.

Macintyre, S.A. (1999), "Magnetic field measurement", in *Webster, J.G. The measurement, instrumentation, and sensors handbook*, Boca Raton, Fla, CRC Press published in cooperation with IEEE Press, pp. 36-18.

NOAA Space Weather Prediction Center, "Satellites and Space Weather", available at: http://www.swpc.noaa.gov/info/Satellites.html (accessed 15 August 2011).

Ogunyanda, K. (2013), A superconducting quantum interference device (SQUID) magnetometer for nanosatellite space weather missions, Unpublished thesis, Cape Peninsula University of Technology, South Africa.

Powersim (2001), "PSIM user manual", available at: http://tec.upc.es/ep/psim-manual.pdf (accessed 26 April 2012).

Star Cryoelectronics (2009), White Paper on HTS magnetometer M1000, Santa Fe.

Texas Instruments (2005), White Paper on Low-noise JFET-input operational amplifiers, Dallas.

Texas Instruments (2008), White Paper on 1.6GHz, low-noise, FET-input operational amplifier. Dallas.

van Zyl, D.S. (2010), "SQUID detected low- field NMR for the evaluation of internal fruit quality", available at: http://scholar.sun.ac.za/handle/10019.1/5208 (accessed 12 March 2012).

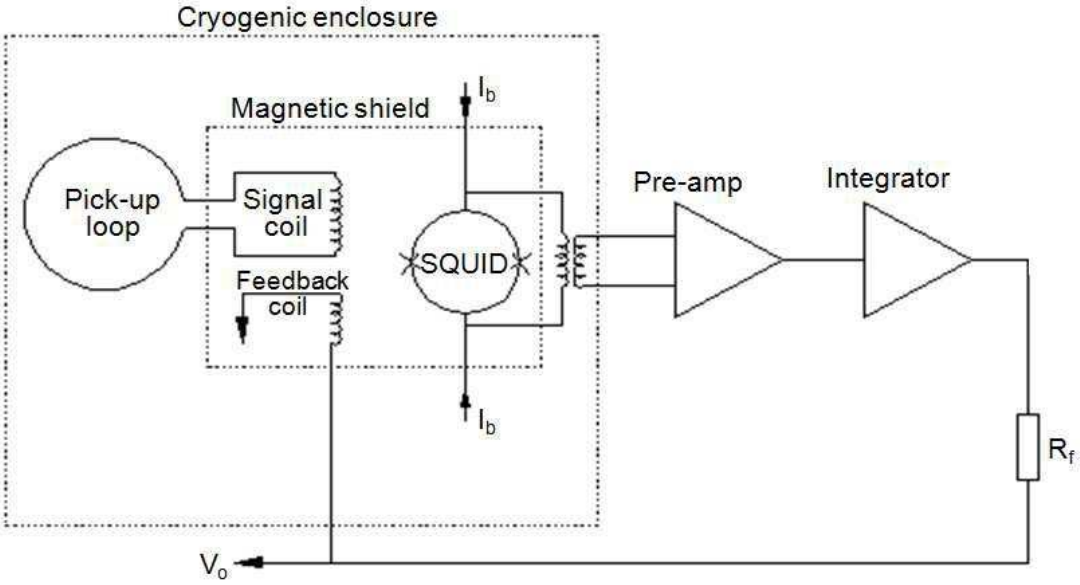

Figure 1: dc SQUID magnetometer operation mode

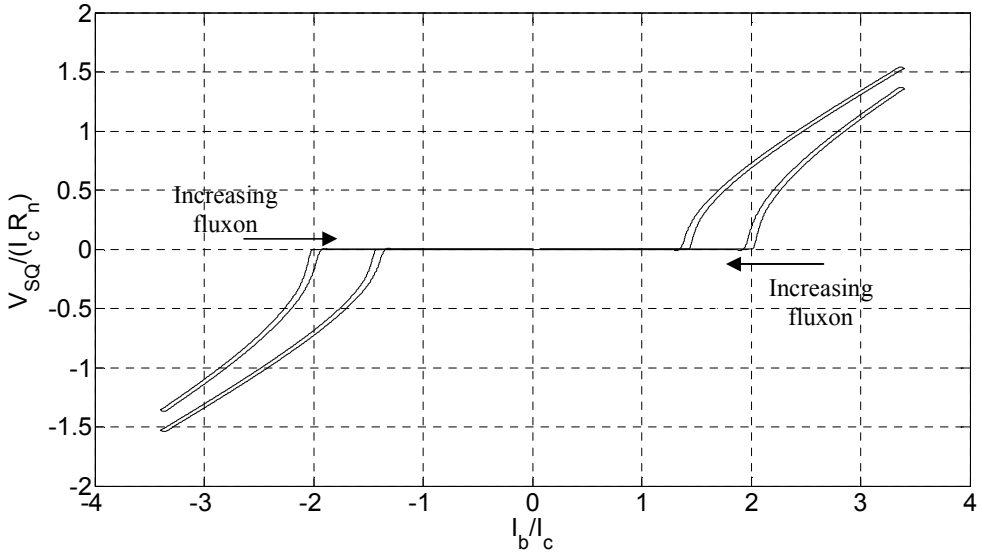

Figure 2: The dc SQUID voltage current characteristics in the order of increasing applied flux, from the extreme sides towards the middle

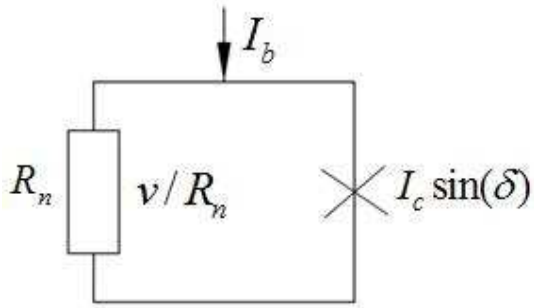

Figure 3: Equivalent circuit of a resistively shunted Josephson junction

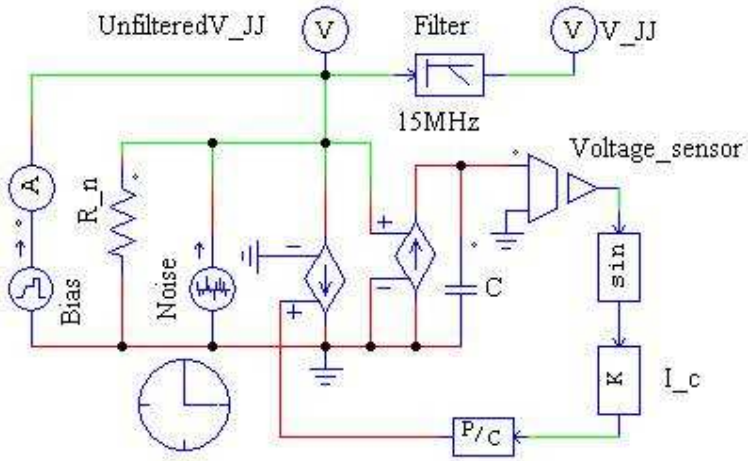

Figure 4: The PSIM model of a RSJ Josephson junction

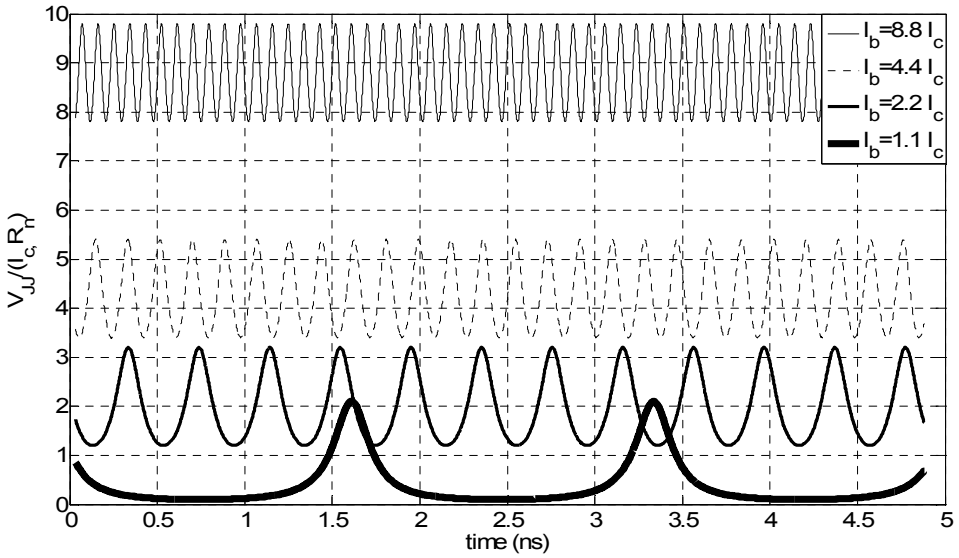

Figure 5: The simulated Josephson junction's oscillations at steady bias currents (I_b = 1.1 I_c, 2.2 I_c, 4.4 I_c and 8.8 I_c)

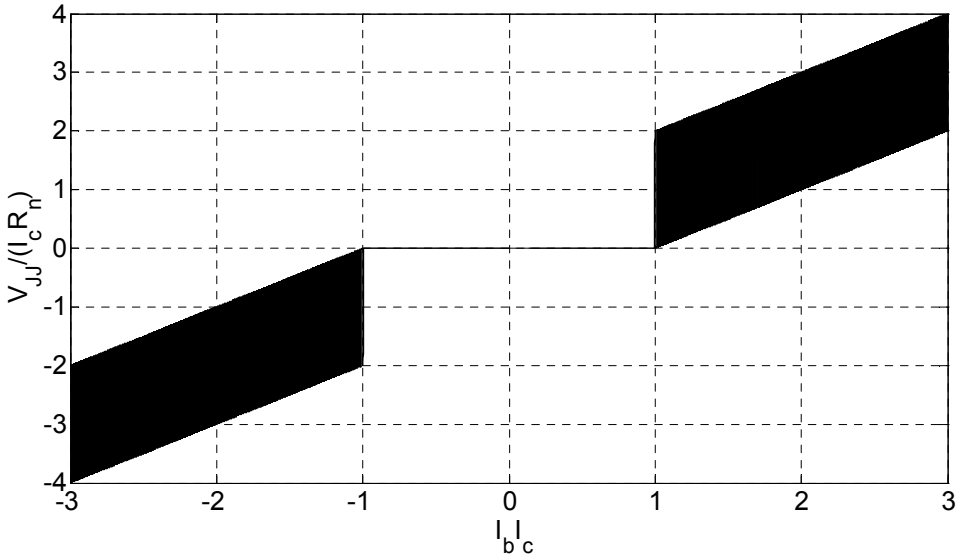

Figure 6: The simulated Josephson junction showing the unfiltered *V -I* characteristics

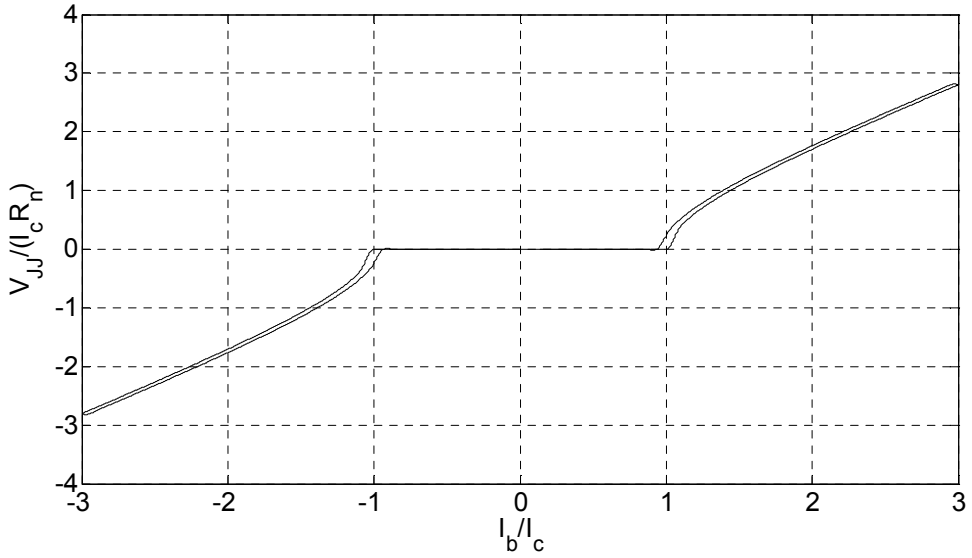

Figure 7: The simulated Josephson junction showing the filtered *V -I* characteristics

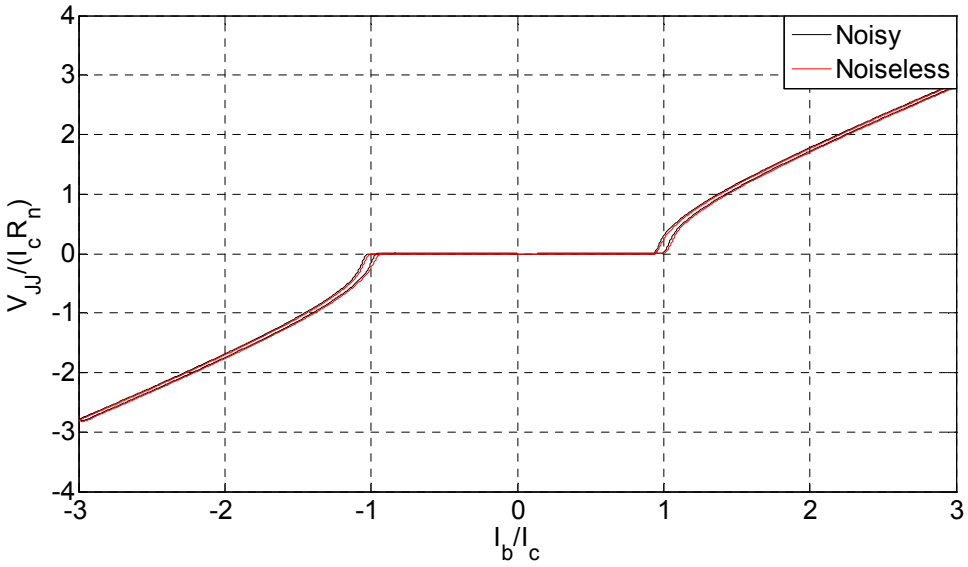

Figure 8: The simulated Josephson junction showing the superimposed *V -I* characteristics, both with and without noise

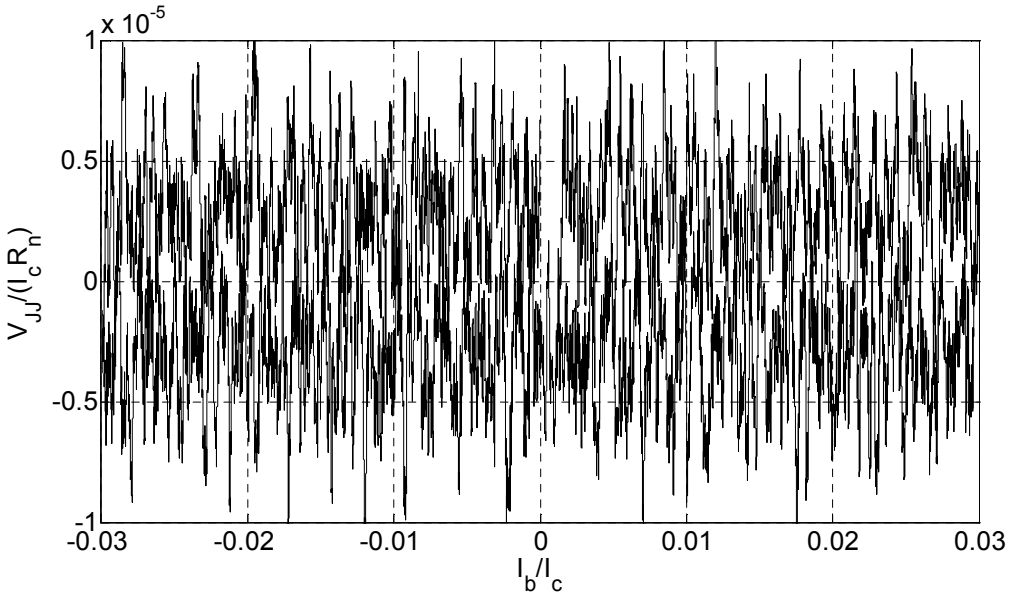

Figure 9: The simulated Josephson junction showing the distorted *V* - *I* characteristics, when the bias current is swept between -0.03 I_c and 0.03 I_c

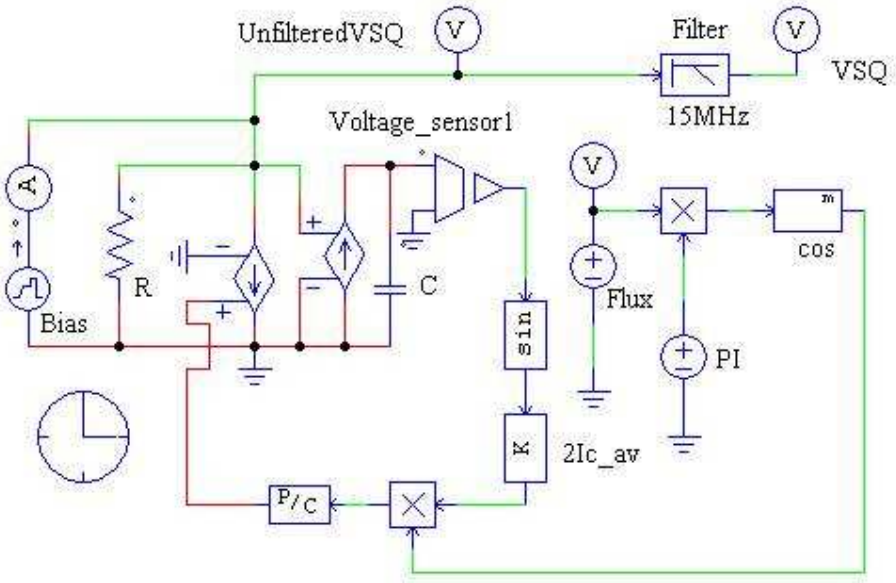

Figure 10: The PSIM model of a dc SQUID magnetometer

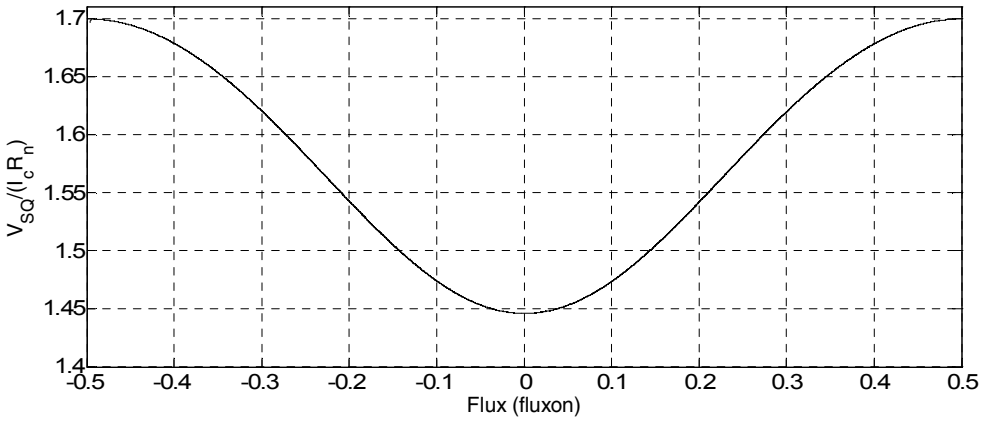

Figure 11: The simulated resistively shunted junction SQUID output voltage-flux response with a swept input of ± 0.5 Φ_0

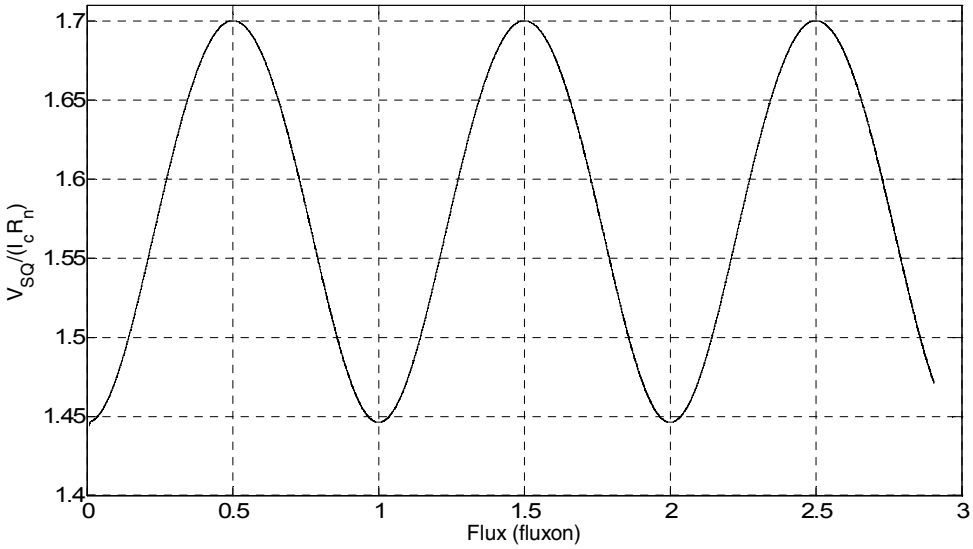

Figure 12: The simulated resistively shunted junction SQUID output voltage-flux response with a 3 Φ_0 sinusoidal input at 5 kHz

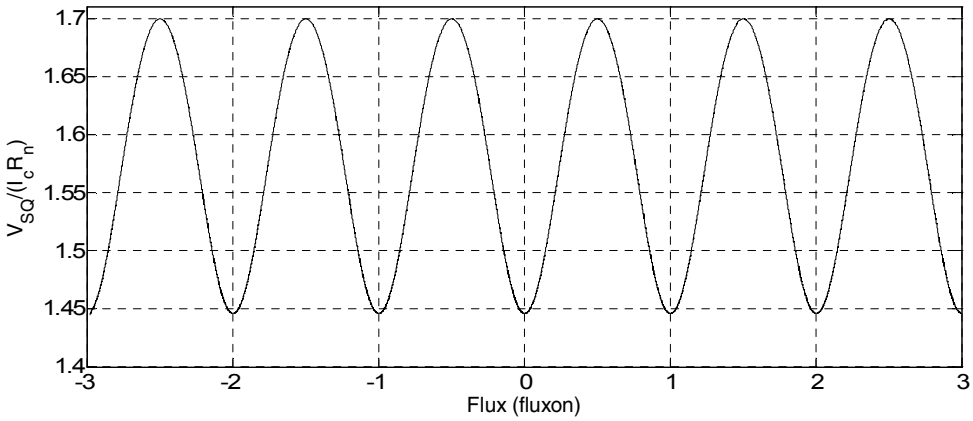

Figure 13: The simulated resistively shunted junction SQUID output voltage-flux response with a swept input of ± 3 Φ_0

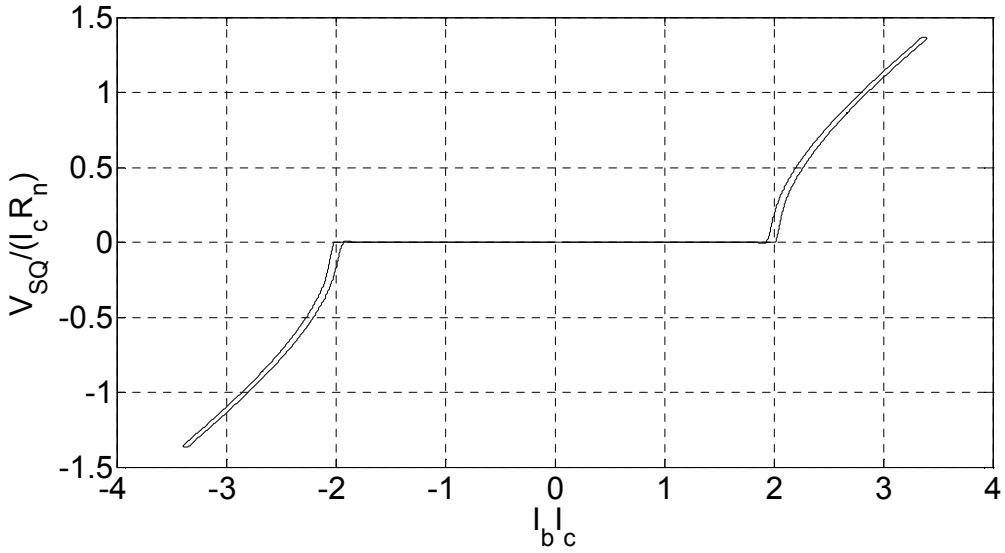

Figure 14: The simulated SQUID's *V* - *I* characteristics at 0 Φ_0 input flux with no noise introduced

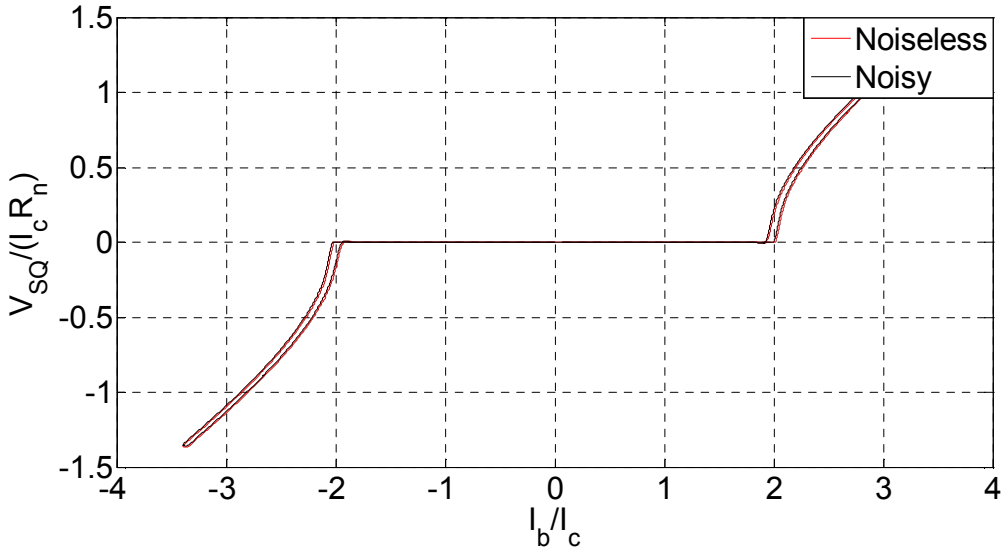

Figure 15: The simulated SQUID's *V* - *I* characteristics at 0 Φ_0 input flux with a 500 MHz bandwidth noise superimposed

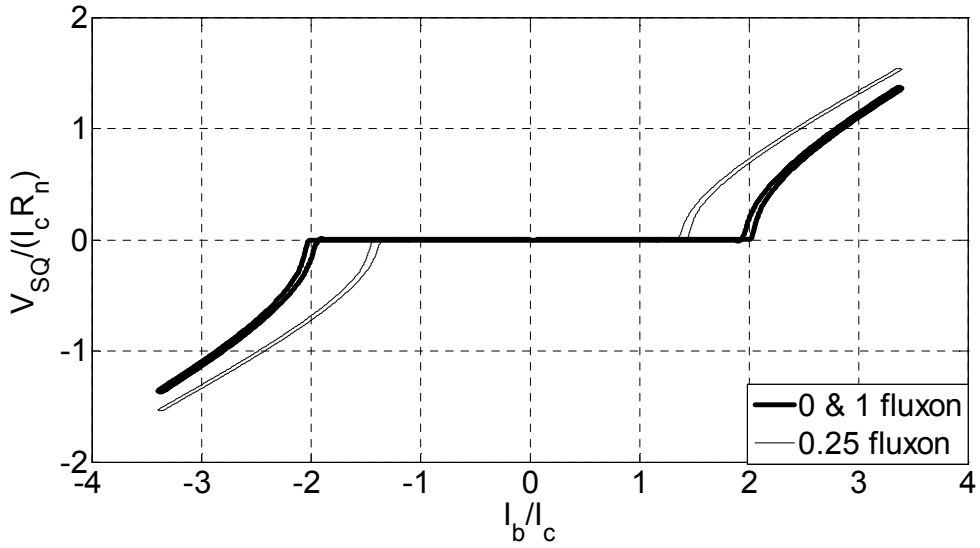

Figure 16: Superimposed SQUID's *V* - *I* characteristics at input fluxes of 0 Φ_0, 0.25 Φ_0 and 1 Φ_0

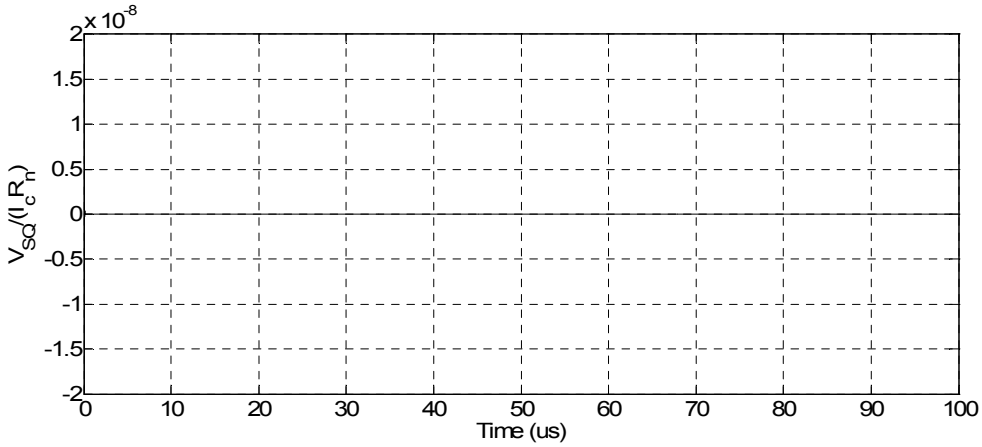

Figure 17: The simulated SQUID's voltage response at I_b = 15 µA bias current

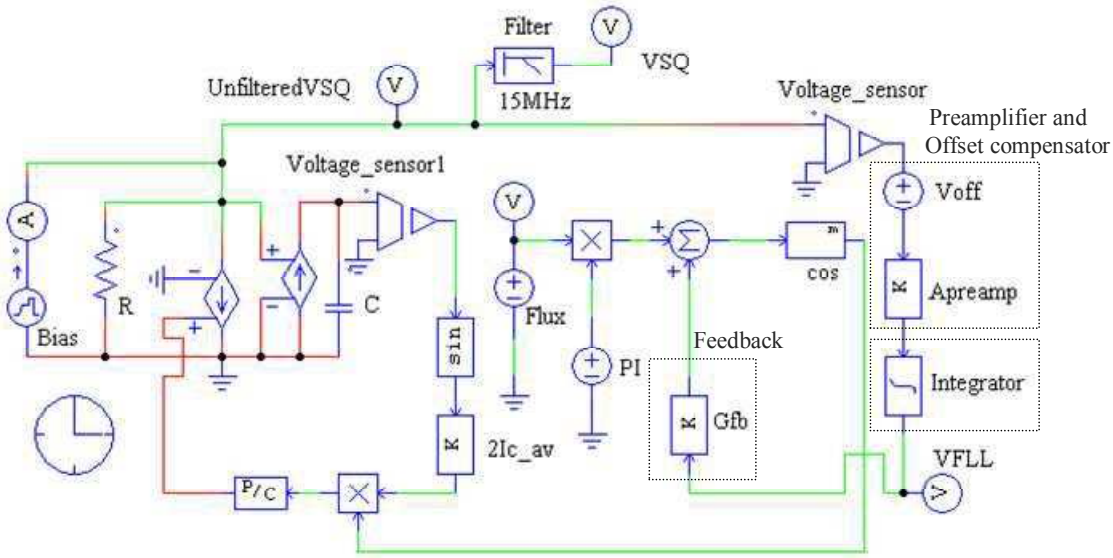

Figure 18: The PSIM model of the flux locked loop

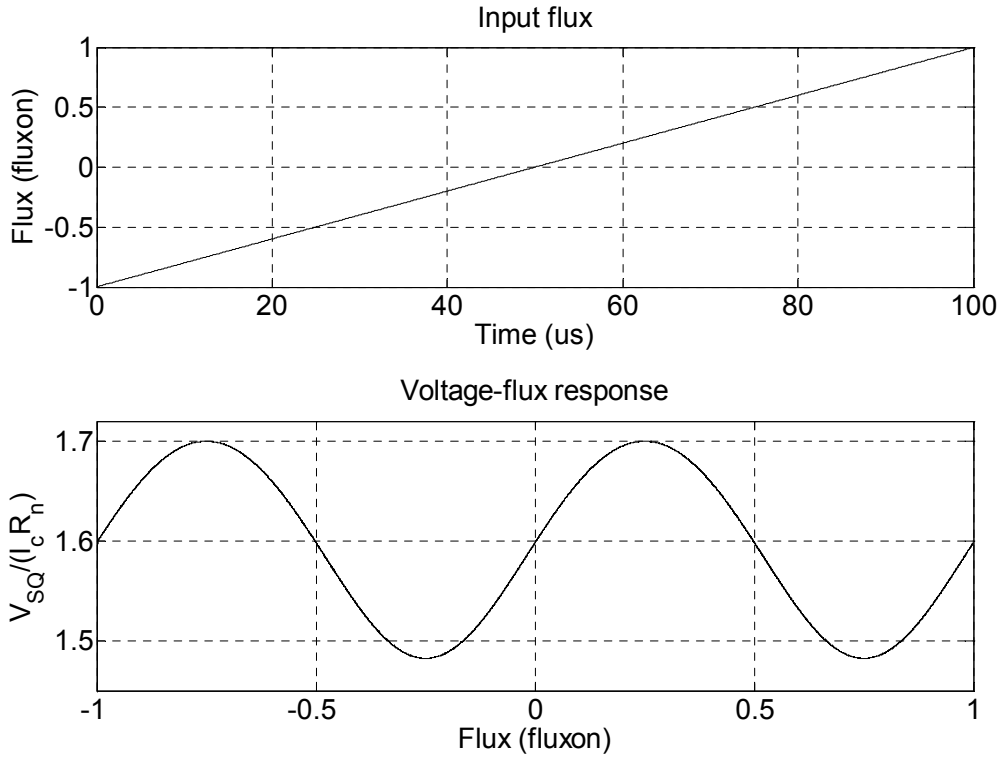

Figure 19: The SQUID's voltage response to a swept input flux from -12.5 Φ_0 to 0.75 Φ_0, without the flux locked loop

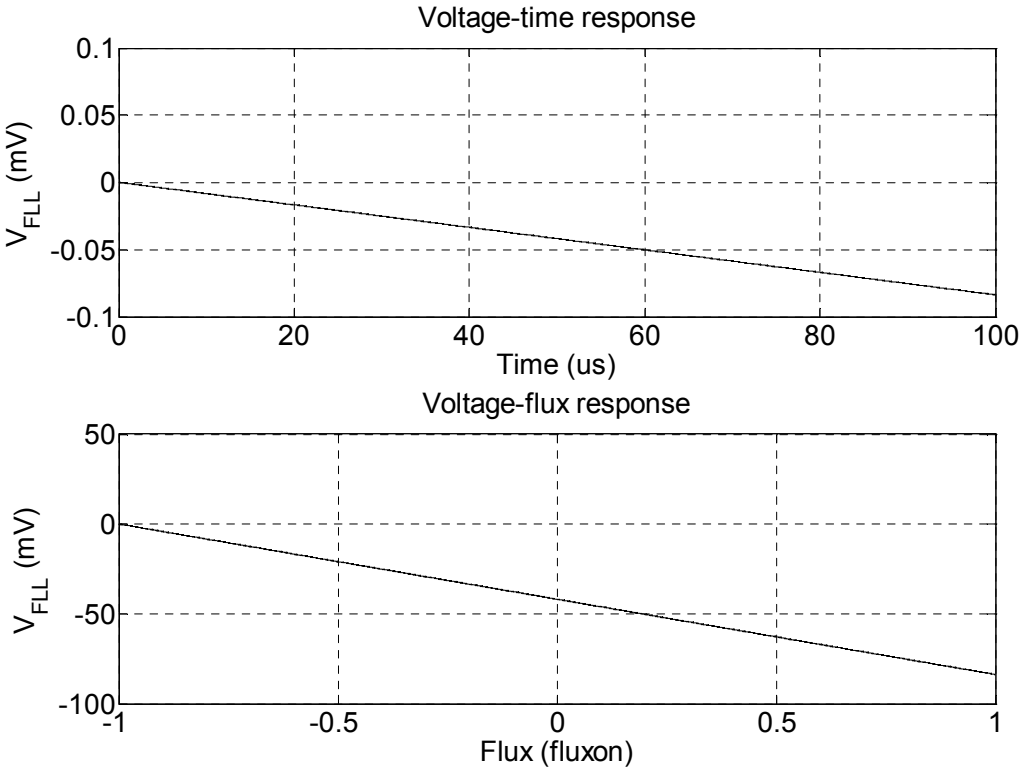

Figure 20: The SQUID's voltage response to a swept input flux from -12.5 Φ_0 to 0.75 Φ_0, using the flux locked loop

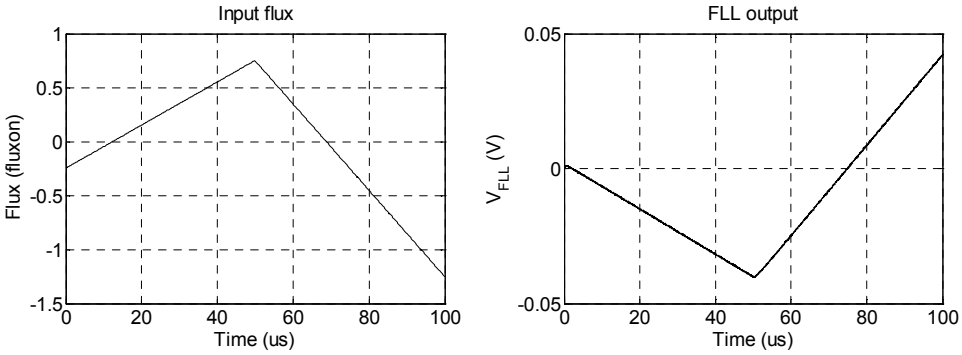

Figure 21: The flux locked loop's voltage response to a swept input flux from - 0.25 Φ_0 to 0.75 Φ_0 and later to – 1.25 Φ_0

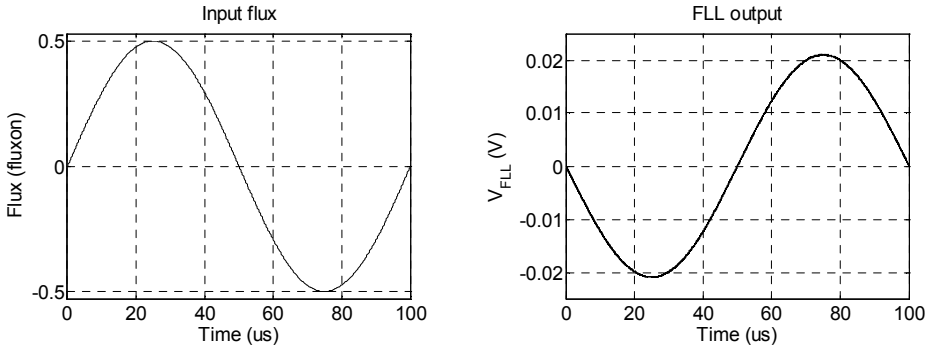

Figure 22: The flux locked loop's voltage response to a sinusoidal input flux of amplitude, 0.5 Φ_0 at 10 kHz